Extensional Flow of Newtonian and Boger Fluids Through a Flow Focusing Microdevice

Mónica S.N. OLIVEIRA [1,*], Fernando T. PINHO [2], Manuel A. ALVES [1]

* Corresponding author: Tel.: +351 225081400 Ext.1209; Fax: +351 225081440; Email: monica.oliveira@fe.up.pt
1: Centro de Estudos de Fenómenos de Transporte, Dep. Eng. Química, Faculdade de Engenharia, Universidade do Porto, Porto, Portugal
2: Centro de Estudos de Fenómenos de Transporte, Dep. Eng. Mecânica, Faculdade de Engenharia, Universidade do Porto, Porto, Portugal

Abstract In this work we perform a numerical and experimental study on the flow of Newtonian and viscoelastic fluids through a microfluidic device in which hydrodynamic flow focusing is produced using two balanced lateral sheath streams that shape a third inlet stream. The flow focusing device used was conceived to achieve a nearly constant extensional rate along the centerline and is shaped much like a conventional cross-slot except for comprising three inlets and one exit channel. The work undertaken comprises experimental flow visualization as well as 2D and 3D numerical calculations using a finite volume method. The Newtonian fluid used in the experiments was distilled water and the viscoelastic fluid was an aqueous solution containing 125 ppm (w/w) of polyacrylamide (PAA, $Mw = 18\times10^6$ g/mol), to which 1% of salt (NaCl) was added. The addition of salt to a shear-thinning PAA solution resulted in a low viscosity Boger fluid, i.e., a viscoelastic fluid with a nearly constant viscosity. The combination of small length scales characteristic of microfluidics with this type of fluid allows us to observe strong elastic effects in the absence of shear-thinning and inertial effects (or at least when these effects are weak). We report a rich variety of flow features, which depend on the fluid used as well as on the operational conditions. Additionally, we show good qualitative agreement between the experimental observations and the numerical predictions.

Keywords: Microfluidics, Flow-focusing, Viscoelasticity, Boger Fluids, Elastic instabilities, Free vortices

1. Introduction

Cross-shaped devices have been used broadly for various different purposes, both as a cross-slot or as a flow focusing device. The use of the flow focusing device at the microscale has already shown great potential in applications that range from passively promoting mixing (e.g. Jensen 1998), a difficult task in microfluidics, to the generation of droplets with controlled shape and size (e.g. Anna and Mayer 2006), or the synthesis of micro particles (e.g. Dendukuri and Doyle 2009).

In particular, the small length scales typical of microfluidic channels (on the order of tens to hundreds of microns) enable the generation of flows with high deformation rates under low inertial conditions (Rodd et al. 2005, Oliveira et al. 2007). The strong elongational flows that can be generated at the center of these devices make them particularly suitable to study extensional effects in complex fluid flows (Arratia et al. 2008; Oliveira et al. 2009). For example, Arratia et al. (2008) studied the effect of elasticity on filament thinning and break-up, using sets of two immiscible fluids, and observed distinct behaviors for Newtonian and polymeric fluids which could be useful in the scope of rheometric purposes. Oliveira et al. (2009) investigated numerically the onset of two distinct elastic instabilities in viscoelastic fluid flows which include the transition to asymmetric but steady flow, and another transition at higher Deborah numbers to unstable flow. This time-dependent elastic instability can be exploited to passively promote mixing at the microscale under low

Reynolds number flow conditions.

In this work, we aim to capture these flow features experimentally and characterize the flow through this type of device, under different flow conditions, using both a Newtonian and a viscoelastic fluid. Furthermore, the results are compared with numerical predictions obtained using our in-house finite volume viscoelastic code.

2. Fluid Characterization and Experimental Techniques

In the experiments we used distilled water and an aqueous solution containing 125ppm (w/w) of polyacrylamide (PAA, $Mw = 18\times10^6$ g/mol), to which 1% of salt (NaCl) was added. The fluids used were characterized rheologically in steady shear using a rotational rheometer (Anton Paar, Physica MCR301) and in extension using a capillary breakup extensional rheometer (Thermo Haake GmbH, CaBER1). The results obtained with the rotational and extensional rheometers are shown in Figure 1. Typically, solutions of long polymer molecules, like those of PAA, exhibit a shear-thinning viscosity. However, the addition of salt results in a PAA solution with a nearly constant shear viscosity ($\eta = 1.31$ mPa s) as shown in Figure 1a while simultaneously exhibiting viscoelasticity. This fluid can, therefore, be considered a low viscosity Boger fluid, which allows us to consider the effects of elastic properties in the absence of other non-Newtonian effects (Campo-Deaño et al. 2011).

The relaxation time was determined using a CaBER experiment in which the fluid is placed between two circular plates (of diameter d_p = 6mm) initially separated by a 2 mm gap and is stretched as the top plate moves to a final gap of 9.4 mm. In the central region between the plates, a cylindrical fluid filament is formed and its diameter starts to thin (cf. Figure 1b) as a result of the competition between viscoelastic and capillary effects. The filament diameter decay near its center is monitored along time (t) using a laser, and the relaxation time (λ) can then be determined by fitting the region of the curve which exhibits an exponential decay to (Entov and Hinch, 1997):

$$\frac{D(t)}{D_0} = C\exp\left(-\frac{t}{3\lambda}\right) \tag{1}$$

where D_0 represents the initial diameter of the filament, and C ia a fluid dependent constant, yielding λ = 12.4 ms.

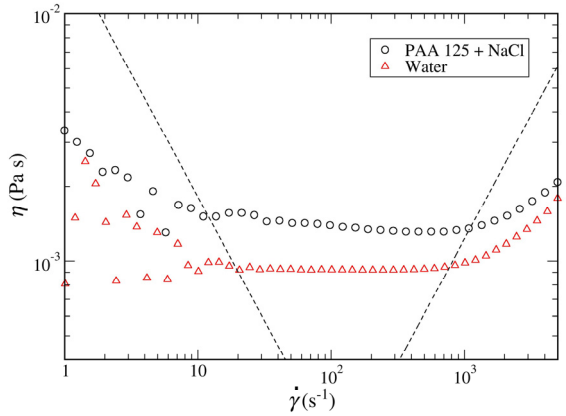

(a)

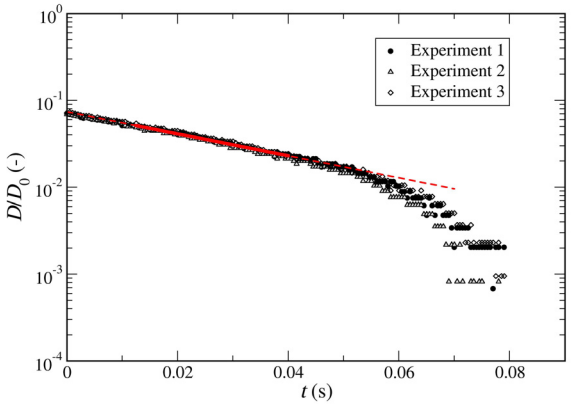

(b)

Figure 1. Fluid Rheology: a) Steady shear-viscosity curves; b) Time evolution of the filament diameter in a CaBER experiment (symbols) and fit to Equation 1 (line). The dotted lines in a) represent the measurable viscosity limits based on 20× the minimum resolvable torque (1×10^{-7} N m) (i), and the onset of inertial instabilities (ii).

The microchannels were fabricated in PDMS (poly(dimethylsiloxane)) using a SU-8 mold by standard soft-lithography techniques.

The channels produced are planar with a constant depth (h) and the width of the inlet and outlet channels (w) is kept the same in order to confer a square cross-section to the geometry ($w \times h = 10^4$ μm^2). The three inlet flow rates are controlled separately using a syringe pump, allowing us to vary the imposed flow rate ratio or the corresponding velocity ratio ($VR = U_2 / U_1$), defined as the ratio of the inlet average velocities in the side streams (U_2) to the average velocity in the central inlet stream (U_1).

Flow visualizations were carried out using streak photography, in which *long* exposures are used to capture the flow patterns. For this purpose, the fluids were seeded with 1 μm fluorescent tracer particles (Ex/Em: 520/580 nm) and the flow was illuminated with a 100 W mercury lamp and visualized using an inverted epi-fluorescence microscope (DMIL LED, Leica Microsystems) equipped with a CCD camera (DFC350 FX, Leica Microsystems GmbH) and appropriate filters (Leica Microsystems GmbH, excitation filter BP 530-545 nm, dichroic 565 nm and barrier filter 610-675 nm).

3. Numerical Method and Governing Equations

An in-house fully-implicit finite volume method (FVM) was used to solve the equations of conservation of mass and momentum:

$$\nabla \cdot \mathbf{u} = 0 \tag{2}$$

$$\rho\left(\frac{\partial \mathbf{u}}{\partial t} + \mathbf{u} \cdot \nabla \mathbf{u}\right) = -\nabla p + \nabla \cdot \boldsymbol{\tau} \tag{3}$$

together with an appropriate constitutive equation for the extra-stress tensor ($\boldsymbol{\tau}$). Here we used the UCM model:

$$\boldsymbol{\tau} + \lambda \overset{\nabla}{\boldsymbol{\tau}} = 2\eta \mathbf{D} \tag{4}$$

In Equations (2)-(4), $\mathbf{u}$ is the velocity vector, $\mathbf{D}$ is the strain rate tensor, p is the pressure, ρ is the fluid density and the symbol $^{\nabla}$ above $\boldsymbol{\tau}$ denotes its upper-convected derivative.

We use an implicit first-order Euler scheme for time discretization, central differences for the discretization of the diffusive terms and a high-resolution scheme for the discretization of the advective terms of the momentum and constitutive equations. More details about the FVM can be found in a series of previous papers (Oliveira et al. 1998, Alves et al. 2003, Afonso et al. 2009) and are not repeated here.

4. Results and Discussion

4.1 Newtonian fluid flow

The flow through the cross-like geometry, in which two opposing lateral fluid streams shape a third inlet stream that is flowing perpendicularly to the lateral entrances, generates a converging flow region (cf. Figure 2) somehow similar to that obtained in a hyperbolic contraction geometry (McKinley et al. 2007, Oliveira et al. 2007). In this geometry, the outline of the converging flow region is defined by a number of operational variables such as the velocity ratio and the Reynolds number (Re). In the case of viscoelastic fluids, the Deborah number (De) is also an important parameter. Here we define the Re and De based on the exit channel variables:

$$Re = \frac{\rho U_3 w}{\eta} \tag{6}$$

$$De = \lambda \frac{U_3}{w} \tag{7}$$

Under the operational conditions illustrated in Figure 2, the flow is steady and symmetric about $x = 0$ and the curvature of the separation streamlines near the lateral entrances is enhanced as VR increases.

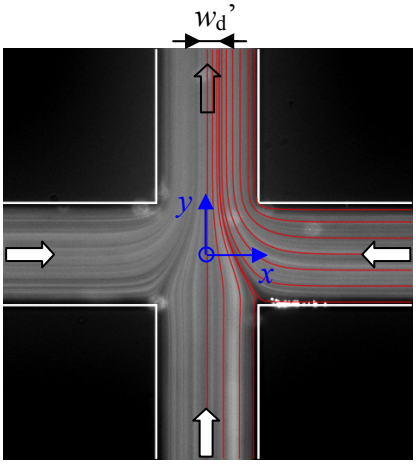

(a) Q_1 = 0.3 ml/h Q_2 = 0.3 ml/h
VR = 1, Re = 2.8

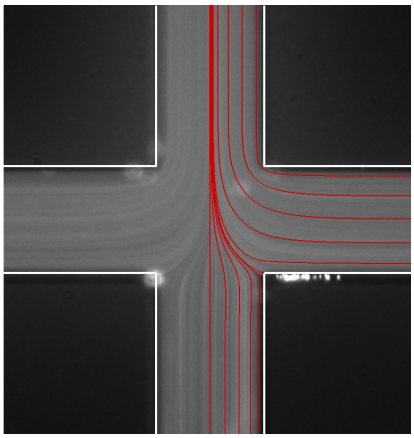

(b) Q_1 = 0.3 ml/h Q_2 = 1.5 ml/h
VR = 5, Re = 1.0×10^{1}

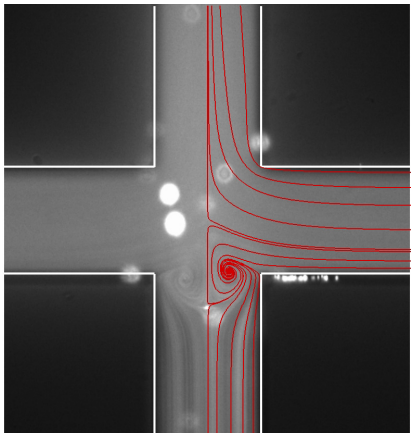

(c) Q_1 = 0.3 ml/h Q_2 = 21 ml/h
VR = 70, Re = 1.3×10^{3}

Figure 2. Water flow patterns at different VR.

One interesting characteristic of the geometry used is that, unlike other micro-devices such as abrupt and smooth contractions (Rodd et al. 2005; McKinley 2007; Oliveira et al. 2007), we can adjust the Hencky strain by varying VR without changing the size and shape of the device. We define the Hencky strain based on the widths of the converging region far upstream (w) and downstream (w_d') of the central region: $\varepsilon_H = \ln(w_d'/w)$, where w_d' is illustrated in Figure 2a. The fact that we are able to tune the Hencky strain by varying only the ratio of flow rates can be very beneficial in experimental terms.

One interesting flow feature observed for Newtonian fluid flow is the appearance of divergent streamlines upstream of the junction despite the hydrodynamic focusing imposed by the lateral sheath streams; followed by the onset and enhancement of symmetrical wall-detached recirculations that form near the centerline (Figure 2c) above a critical value of the ratio of inlet average velocities. We were able to show numerically that free vortex formation occurs even under creeping flow conditions, but that inertia accelerates its appearance. In contrast, the presence of the walls in three-dimensional geometries has a stabilizing effect, delaying the onset of these free recirculations.

4.1 Boger fluid flow

The effect of De on the flow patterns under creeping flow conditions has been studied numerically in a previous paper using different constitutive models (Oliveira et al. 2008). The results obtained with the UCM model show that, at low Deborah numbers, the flow is symmetric relative to the centerline. Strong viscoelastic effects were observed as the Deborah number increased and the flow was seen to become asymmetric, while remaining steady, for De above a critical value. Above an even higher threshold value of the Deborah number, a subsequent instability was identified in which the flow becomes unsteady. For very low VR, the flow evolves directly from steady symmetric to unsteady, oscillating in time without ever going through the intermediate regime of steady asymmetric flow, since the normal stresses are not sufficiently high to trigger this intermediate transition.

As a consequence of the small length scales and high deformation rates associated with microfluidic flows, we were able to observe experimentally the transition to steady asymmetric flow using the Boger fluid, as shown in Figure 3. This transition is driven by elastic normal stresses that act along the streamlines and is entirely absent in the corresponding Newtonian fluid flow.

Numerically, we were able to capture qualitatively the experimental flow patterns using simplified 2D calculations (compare Figures 3 and 4). In particular, when the flow rate in the lateral entrances is increased and the onset of asymmetric flow is observed, the size and shape of the experimental asymmetry is in good agreement with the numerical predictions. However, in the numerical results, recirculations near the top walls of the lateral channels are observed which are not visible in the experiments under equivalent conditions. Nevertheless, these numerical calculations are a good starting point and we expect that, using a more suitable constitutive equation and 3D calculations, we will be able to provide predictions which are more realistic in quantitative terms.

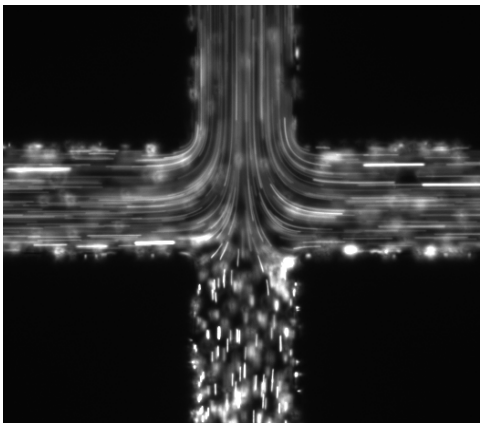

(a) Q_1 = 0.01 ml/h Q_2 = 0.05 ml/h
VR = 5, Re = 0.23, De = 0.38

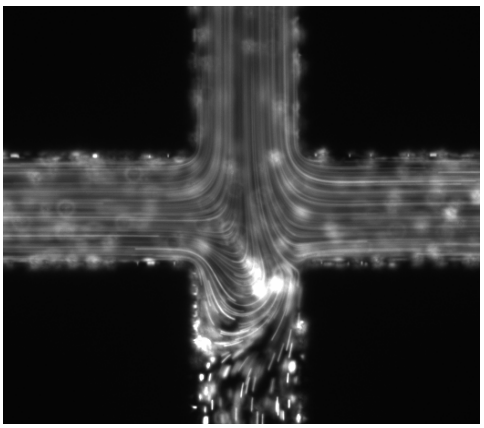

(b) Q_1 = 0.01 ml/h Q_2 = 0.2 ml/h
VR = 20, Re = 0.87, De = 1.41

Figure 3. Experimental flow patterns of the viscoelastic fluid: (a) symmetric flow; (b) asymmetric steady flow.

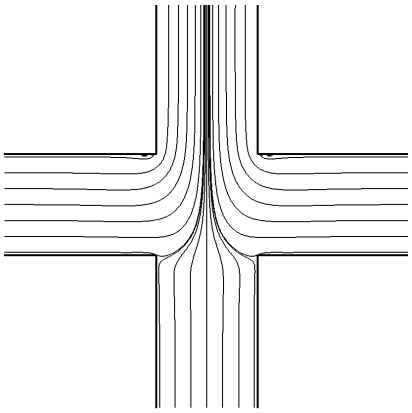

(a) Q_1 = 0.01 ml/h Q_2 = 0.05 ml/h
VR = 5, Re = 0.23, De = 0.38

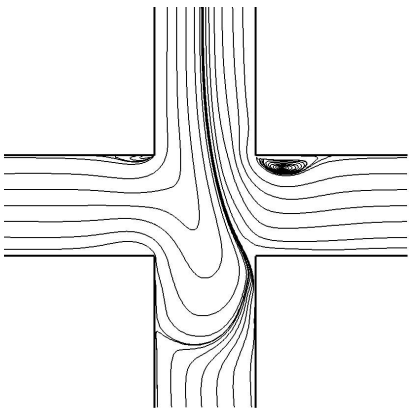

(b) Q_1 = 0.01 ml/h Q_2 = 0.2 ml/h
VR = 20, Re = 0.87, De = 1.41

Figure 4. Flow patterns obtained in 2D numerical calculations for the UCM fluid: (a) symmetric flow; b) asymmetric steady flow.

Acknowledgements:
We thank FCT, FEDER and COMPETE for financial support through projects REEQ/262/EME/2005, REEQ/928/EME/2005 and PTDC/EME-MFE/099109/2008.

References

Afonso A.M., Oliveira P.J., Pinho F.T., Alves M.A., 2009. The log-conformation tensor approach in the finite-volume method framework, J. Non-Newt. Fluid Mech. 157, 55-65.

Alves M.A., Pinho F.T., Oliveira P.J., 2000. Effect of a high-resolution differencing scheme on finite-volume predictions of viscoelastic flows, J. Non-Newton. Fluid Mech. 93, 287-314.

Anna S.L. and Mayer H.C., 2006. Microscale tipstreaming in a microfluidic flow, Phys. Fluids 18, 121512 1-13.

Arratia P.E., Gollub J.P., Durian D.J., 2008. Polymeric filament thinning and breakup in microchannels, Phys. Rev. E 77, 036309 1-6.

Campo-Deaño L., Galindo-Rosales F.J., Pinho, F.T., Alves M.A., Oliveira M.S.N., 2011. Flow of low viscosity Boger fluids through a microfluidic hyperbolic contraction, J. Non-Newton. Fluid Mech., *Submitted*.

Dendukuri D. and Doyle P.S., 2009. The synthesis and assembly of polymeric microparticles using microfluidics, Adv. Mater. 21, 1–16.

Entov V.M. and Hinch E.J., 1997. Effect of a spectrum of relaxation times on the capillary thinning of a filament of elastic liquid. J. Colloid Interface Sci. 72, 31-51.

Jensen K., 1998. Chemical kinetics: smaller, faster chemistry, Nature 393, 735–737.

McKinley G.H., Rodd L.E., Oliveira M.S.N., Cooper-White J.J., 2007. Extensional Flows of Polymer Solutions in Microfluidic Converging/Diverging Geometries, J. of Central South Univ. of Technol. 14, 6-9.

Oliveira P.J., Pinho F.T., Pinto G.A., 1998. Numerical simulation of non-linear elastic flows with a general collocated finite-volume method, J. Non-Newton. Fluid Mech. 79, 1-43.

Oliveira M.S.N., Alves M.A., McKinley G.H., Pinho F.T., 2007. Viscous flow through microfabricated hyperbolic contraction, Exp. Fluids 43, 437–451.

Oliveira M.S.N., Rodd L.E., McKinley G.H., Alves M.A., 2008. Simulations of extensional flow in microrheometric devices, Microfluid. Nanofluid. 5, 809–826.

Oliveira M.S.N., Pinho F.T., Poole R.J., Oliveira P.J., Alves M.A., 2009. Purely elastic flow asymmetries in flow-focusing devices, J. Non-Newton. Fluid Mech.160, 31-39.

Rodd L.E., Scott T.P., Boger D.V., Cooper-White J.J., McKinley G.H., 2005. The inertio-elastic planar entry flow of low-viscosity elastic fluids in micro-fabricated geometries, J. Non-Newton. Fluid Mech. 129, 1–22.